Inorg. Chem. **2005**, *44*, 6415–6424

Investigating Bidentate and Tridentate Carbamoylmethylphosphine Oxide Ligand Interactions with Rare-Earth Elements Using Electrospray Ionization Quadrupole Ion Trap Mass Spectrometry

Matthew C. Crowe,[†] Ramesh N. Kapoor,[‡] Francisco Cervantes-Lee,[‡] Laszlo Párkányi,[‡] Louis Schulte,[§] Keith H. Pannell,*[,‡] and Jennifer S. Brodbelt*[,†]

Department of Chemistry and Biochemistry, The University of Texas at Austin, Austin, Texas 78712, Department of Chemistry, The University of Texas at El Paso, El Paso, Texas 79968, and Actinide Chemistry Process Group, Los Alamos National Laboratory, Los Alamos, New Mexico 87545

Received February 28, 2005

Electrospray ionization (ESI) quadrupole ion trap mass spectrometry (QIT-MS) and collisionally activated dissociation (CAD) were used to evaluate the rare-earth binding properties of two hydrophobic carbamoylmethylphosphine oxide (CMPO) ligands, the normal bidentate variety, $(t\text{-BuC}_6\text{H}_4)_2\text{P(O)CH}_2\text{C(O)N}(i\text{-Bu})_2$ (**A**), a new potentially tridentate extractant, $(t\text{-BuC}_6\text{H}_4)_2\text{P(O)CH[CH}_2\text{C(O)N}(i\text{-Bu})_2\text{]C(O)N}(i\text{-Bu})_2$ (**B**), and tributyl phosphate. The mass spectral results obtained from analysis of 1% HNO_3/methanol solution containing the ligands and dissolved lanthanide salts reveal that the favorable stoichiometries of the ligand/metal/nitrate complexes are 2:1:2 for the bidentate ligand **A**, 1:1:2 for the tridentate ligand **B**, and 3:1:2 for the monodentate tributyl phosphate. These observed stoichiometries correlate with the number of available binding sites on each ligand as well as with potential steric effects. Energy-variable collisionally activated dissociation experiments showed that for the 2:1:2 complexes involving ligand **A** or **B**, as the ionic radius of the bound metal decreased, the removal of nitric acid required less energy and resulted in less extensive spontaneous solvent coordination. This experimental trend suggests that, as the ionic radius of the lanthanide ion decreases, a pair of the carbamoylmethylphosphine ligands is able to more completely solvate the bound metal ion thereby weakening the nitrate–metal interaction.

Introduction

Nuclear waste reprocessing requires the nearly quantitative recovery of uranium and plutonium from fission products, such as *trans*-uranium (TRU) actinides and lanthanides, and safe disposal of the radioactive fission products.[1−4] The first stage in nuclear fuel reprocessing introduces high concentrations (3−4 M) of nitric acid to solubilize uranium oxide.[4,5] Subsequent reprocessing involves the liquid−liquid extraction of uranium(VI) and plutonium(IV) from the aqueous waste streams with tributyl phosphate diluted in some type of aliphatic hydrocarbon mixture and is known as the PUREX (plutonium and uranium reduction extraction) process.[2−6] After this extraction, the radioactive *trans*-uranium (TRU) actinides still in the aqueous effluate can be separated from the stable lanthanide ions via the TRUEX (*trans*-uranium extraction) process.[3,4,6,7] This can be accomplished with several different types of ligands, and many have been designed and studied to increase the effectiveness of this process.[3,6−12] Given the highly acidic extraction

* To whom correspondance should be addressed. E-mail: jbrodbelt@mail.utexas.edu (J.S.B.), kpannell@utep.edu (K.H.P.).
† The University of Texas at Austin.
‡ The University of Texas at El Paso.
§ Los Alamos National Laboratory.

(1) Murray, R. L. *Nuclear Energy: An Introduction to the Concepts, Systems, and Applications of Nuclear Processes*, 5th ed.; Butterworth Heinemann: Boston, MA, 2001.
(2) Sood, D. D.; Patil, S. K. *J. Radioanal. Nucl. Chem.* **1996**, *203*, 547−573.
(3) Mathur, J. N.; Murali, M. S.; Nash, K. L. *Solvent Extr. Ion Exch.* **2001**, *19*, 357−390.
(4) Paiva, A. P.; Malik, P. *J. Radioanal. Nucl. Chem.* **2004**, *261*, 485−496.
(5) Musikas, C.; Schulz, W. W. In *Principles and Practices of Solvent Extraction*; Rydberg, J., Musikas, C., Choppin, G. R., Eds.; Marcel Dekker Inc.: New York, 1992; p 413.
(6) Eccles, H. *Solvent Extr. Ion Exch.* **2000**, *18*, 633−654.
(7) Schulz, W. W.; Horwitz, E. P. *Sep. Sci. Technol.* **1988**, *23*, 1191−1210.
(8) Drew, M. G. B.; Guillaneux, D.; Hudson, M. J.; Iveson, P. B.; Russell, M. L.; Madic, C. *Inorg. Chem. Commun.* **2001**, *4*, 12−15.

10.1021/ic0503028 CCC: $30.25
Published on Web 08/02/2005

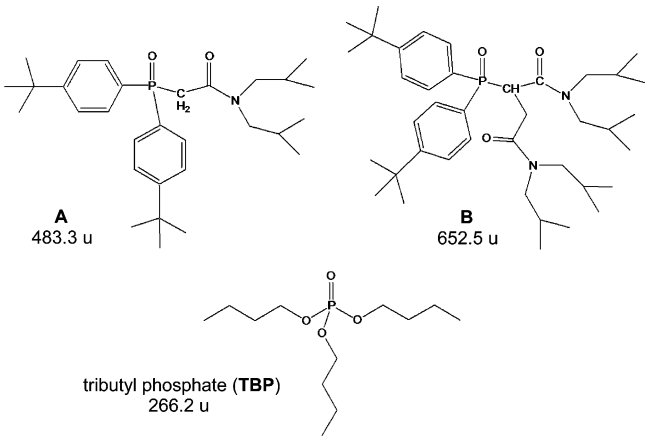

Figure 1. Structures of ligands with molecular weights.

environment and the very similar ionic radii and chemical properties of the lanthanides and actinides, the design of ligands that differentiate via metal−ligand interactions is difficult.[13]

Carbamoylmethylphosphine oxide (CMPO) ligands, $R_2P(O)CH_2C(O)NR'_2$, were developed with a goal of reducing the amount of necessary extractant and volume waste generated in the *trans*-uranium extraction process. In this report, we focus on the study of a very hydrophobic CMPO ligand, $(p\text{-}t\text{-}BuC_6H_4)_2P(O)CH_2C(O)N(i\text{-}Bu)_2$ (**A**) (Figure 1), which has been applied at Los Alamos National Laboratory in a hydrochloric acid version of the TRUEX process and tested for similar use in nitric acid separations.[13] In addition, we investigated a new, potentially tridentate, derivative of **A** in which a second carbamoyl group, $(p\text{-}t\text{-}BuC_6H_4)_2P(O)CH(CH_2C(O)N(i\text{-}Bu)_2)C(O)N(i\text{-}Bu)_2$ (**B**), has been introduced (Figure 1). Furthermore, because the modified TRUEX process uses tributyl phosphate as an additive to the CMPO ligands, we also evaluated this ligand.

There is extensive literature of the use of the CMPO ligands for separations and extractions of lanthanide ions.[14−16] There are several structures illustrating modes of lanthanide−CMPO binding in which predominantly bidentate binding (via P═O and C═O groups) is observed;[17,18] but, monodentate systems in which the CO group is not directly bound to the metal ions are also known.[18] Quantum mechanical calculations have modeled the metal−ligand interactions responsible for such properties and shown that the energy difference between the two forms, mono- and bidentate, are not large but increase in the sequence of La ions from La^{3+} to Yb^{3+}.[19] In general, two molecules of the CMPO lanthanide ions are found in the resulting complexes.

The evaluation of metal−ligand interactions with mass spectrometry has been very successful since the advent of electrospray ionization (ESI), which has the ability to preserve and transport ligand−metal complexes from solution to the gas phase.[20] ESI mass spectrometry (ESI-MS) has been applied to numerous investigations of host−guest complexation and to the general field of molecular recognition.[21−27] This research involved investigations of the stoichiometries, relative stabilities, and conformations of peptide/protein substrate,[21,22] DNA drug,[23,24] and macrocycle/metal complexes.[25−28] Furthermore, several studies have related the results of ESI mass spectrometry experiments to the original solution concentrations, binding interactions, and equilibria active in molecular recognition.[28−40]

The exploration of metal−ligand complexes in the gas phase by ESI-MS has expanded in recent years. Vachet and co-workers have demonstrated that gas-phase ligand addition reactions can be used to probe the gas-phase coordination structures of metal−ligand complexes involving synthetic ligands[41−49] as well as to study copper−protein binding sites in metalloproteins.[50,51] For example, they have used ESI-

(9) Drew, M. G. B.; Guillaneux, D.; Hudson, M. J.; Iveson, P. B.; Madic, C. *Inorg Chem Commun.* **2001**, *4*, 462−466.
(10) Iveson, P. B.; Riviere, C.; Guillaneux, D.; Nierlich, M.; Thuery, P.; Ephritikhine, M.; Madic, C. *Chem. Commun.* **2001**, 1512−1513.
(11) Kolarik, Z.; Mullich, U.; Gassner, F. *Solvent Extr. Ion Exch.* **1999**, *17*, 23−32.
(12) Kolarik, Z.; Mullich, U.; Gassner, F. *Solvent Extr. Ion Exch.* **1999**, *17*, 1155−1170.
(13) Schulte, L. D.; McKee, S. D.; Salazar, R. R. *DOE Spent Nuclear Fuel & Fissile Material Management*; American Nuclear Society, Inc.: La Grange Park, IL, 1996.
(14) Fu, S. S.; Teramoto, M.; Matsuyama, H. *Sep. Sci. Technol.* **2004**, *39*, 517−538.
(15) Nakashima, K.; Kuboto, F.; Maruyama, T.; Goto, M. *Ind. Eng. Chem. Res.* **2005**, *44*, 4368−72.
(16) Turanov, A. N.; Karandashev, V. K.; Yarkevich, A. N.; Kharitonov, A. V.; Safronova, Z. V. *Radiochemistry (Moscow, Russ. Fed.)* **2002**, *44*, 559−564.
(17) (a) Bowen, S. M.; Duessler, E. N.; Paine, R. T. *Inorg. Chem.* **1982**, *21*, 261−267. (b) Caudels, L. J.; Deussler, E. N.; Paine, R. T. *Inorg. Chem.* **1985**, *24*, 441−446.
(18) Bowen, S. M.; Duessler, E. N.; Paine, R. T. *Inorg. Chim. Acta* **1982**, *61*, 155−166.
(19) Boehme, C.; Wipff, G. *Inorg. Chem.* **2002**, *41*, 727−737.
(20) Fenn, J. B.; Mann, M.; Meng, C. K.; Wong, S. F.; Whitehouse, C. M. *Science* **1989**, *246*, 64−71.
(21) Loo, J. A. *Int. J. Mass Spectrom.* **2000**, *200*, 175−186.
(22) Loo, J. A. *Mass Spec. Rev.* **1997**, *16*, 1−23.
(23) Beck, J. L.; Colgrave, M. L.; Ralph, S. F.; Sheil, M. M. *Mass Spec. Rev.* **2001**, *20*, 61−87.
(24) Hofstadler, S. A.; Griffey, R. H. *Chem. Rev.* **2001**, *101*, 377−390.
(25) Young, D. S.; Hung, H. Y.; Liu, L. K. *Rapid Commun. Mass Spectrom.* **1997**, *11*, 769−773.
(26) Brodbelt, J. S. *Int. J. Mass Spectrom.* **2000**, *200*, 57−69.
(27) Schalley, C. A. *Int. J. Mass Spectrom.* **2000**, *194*, 11−39.
(28) Sherman, C. L.; Brodbelt, J. S. *Anal. Chem.* **2003**, *75*, 1828−1836.
(29) Tang, L.; Kebarle, P. *Anal. Chem.* **1993**, *65*, 3654−3668.
(30) Zook, D. R.; Bruins, A. P. *Int. J. Mass Spectrom.* **1997**, *162*, 129−147.
(31) Ikonomou, M. G.; Blades, A. T.; Kebarle, P. *Anal. Chem.* **1990**, *62*, 957−967.
(32) Cech, N. B.; Enke, C. G. *Mass Spectrom. Rev.* **2001**, *20*, 362−387.
(33) Constantopoulos, T. L.; Jackson, G. S.; Enke, C. G. *Anal. Chim. Acta* **2000**, *406*, 37−52.
(34) Sjoberg, P. J. R.; Bokman, C. F.; Bylund, D.; Markides, K. E. *J. Am. Soc. Mass Spectrom.* **2001**, *12*, 1002−1010.
(35) Wang, G. D.; Cole, R. B. *Anal. Chem.* **1994**, *66*, 3702−3708.
(36) King, R.; Bonfiglio, R.; Fernandez-Metzler, C.; Miller-Stein, C.; Olah, T. *J. Am. Soc. Mass Spectrom.* **2000**, *11*, 942−950.
(37) Constantopoulos, T. L.; Jackson, G. S.; Enke, C. G. *J. Am. Soc. Mass Spectrom.* **1999**, *10*, 625−634.
(38) Cole, R. B. *J. Mass Spectrom.* **2000**, *35*, 763−772.
(39) Tang, L.; Kebarle, P. *Anal. Chem.* **1991**, *63*, 2709−2715.
(40) Enke, C. G. *Anal. Chem.* **1997**, *69*, 4885−4893.
(41) Vachet, R. W.; Hartman, J. A. R.; Callahan, J. H. *J. Mass Spectrom.* **1998**, *33*, 1209−1225.
(42) Vachet, R. W.; Challahan, J. H. *J. Mass Spectrom.* **2000**, *35*, 311−320.
(43) Vachet, R. W.; Hartman, J. A. R.; Gertner, J. W.; Callahan, J. H. *Int. J. Mass Spectrom.* **2001**, *204*, 101−112.
(44) Combariza, M. Y.; Vachet, R. W. *J. Am. Soc. Mass Spectrom.* **2002**, *13*, 813−825.
(45) Combariza, M. Y.; Vachet, R. W. *Anal. Chim. Acta* **2003**, *496*, 233−248.

MS to show an elegant correlation between the reactivity of metal complexes with organic ligands in the gas phase and the coordination numbers of the metals.[41−49] The correlation was based on the occurrence or lack of reactions between the metal complexes and various molecules, such as CH_3CN, H_2O, CH_3OH, NH_3, and pyridine. Van Stipdonk et al. have used ESI-MS extensively to examine the complexation of uranyl ions with organic ligands, such as acetone, methanol, H_2O, and 2-propanol, and subsequent dissociation of the resulting multiligated complexes.[52−56] Spontaneous solvation of the resulting multiligated complexes in the gas phase was observed in some cases. This solvation depended on the charge state and stoichiometry of the complexes and was related in part to the coordination number of the uranyl ion.[52−57] In addition, ESI-MS has been applied to evaluate the formation of gas-phase complexes involving rare-earth metal ions and synthetic ligands, along with associated counterions and/or solvent molecules.[58−71] Many groups have used ESI-MS, along with other techniques, as a tool to evaluate the binding characteristics of ligands following their synthesis,[63−65,67] whereas others have studied gas-phase reactions between rare-earth metal ions and volatilized organic ligands in trapping mass spectrometers.[62,69] Recently, the Colette group used ESI-MS to study the stoichiometries and relative stabilities of various 2,6-bis(5,6-dialkyl-1,2,4-triazin-3-yl)pyridine (DATP) ligands with trivalent lanthanide ions.[69,70] In addition, the kinetic stabilities of these complexes were studied via energy-resolved collisional activation, providing useful binding and structural information.[70] This work, along with theoretical studies,[19,72−74] has provided valuable insight into binding modes, stoichiometries, and relative energies of rare-earth/ligand complexes.

The present work describes the application of ESI-MS and collisionally activated dissociation (CAD) tandem mass spectrometry experiments in an effort to obtain an understanding of the relative binding affinities and stoichiometries of carbamoylmethylphosphine oxide and tributyl phosphate ligands with rare-earth ions (La^{3+}−Lu^{3+}) in the gas phase.

Experimental Section

Materials. The di(*tert*-butylphenyl)-*N*,*N*-diisobutylcarbamoylmethylphosphine oxide ligand (**A**) was synthesized using a recently published procedure.[75] The synthesis of ligand **B** is outlined below. Tributyl phosphate and the lanthanide salts were purchased from Aldrich Chemicals (St. Louis, MO) and used without further purification.

Synthesis of $(t\text{-}BuC_6H_4)_2P(O)CH[CH_2C(O)N(i\text{-}Bu)_2]C(O)N(i\text{-}Bu)_2$, B. To a 100 mL THF solution of 4.84 g (10 mmol) of CMPO **A**, in a 250-mL round-bottomed flask, was added 0.25 g (20 mmol) of powdered NaH under an atmosphere of Ar. The mixture was stirred at room temperature for 3 h and then filtered under Ar. To the filtrate was added dropwise 2.06 g (10 mmol) of $ClCH_2C(O)N(i\text{-}Bu_2)$, and the resulting mixture was stirred overnight. Removal of the solvent yielded a white solid that was recrystallized from hexane to produce **B** in 50% yield, 3.3 g (5 mmol).

Analysis for $C_{40}H_{65}PO_3N_2$ (Galbraith Laboratories). Anal. Calcd: C, 73.6; H, 10.03; N, 4.28. Found: C, 73.0; H, 9.95; N, 4.24. Mp: 156−8 °C. IR (cm^{-1}, THF): C(O) 1649 (bd), P(O) 1197. ^{31}P NMR (ppm, $CDCl_3$): 32.1. ^{13}C NMR (ppm, $CDCl_3$): 171.06 (PC*C*O, d, $^2J_{C-P}$ = 15.76 Hz), 170.108 (PCC*C*O, d, J_{C-P} = 2.1 Hz), 155.959 (*para-C*, d, J_{C-P} = 2.56 Hz), 132.89 (*meta-C*, d, J_{C-P} = 9.2 Hz), 132.46 (*meta-C*, d, J_{C-P} = 9.4 Hz), 129.75 (*ipso-C*, J_{C-P} = 100.9 Hz), 128.79 (*ipso-C*, J_{C-P} = 100.9 Hz), 126.33 (*ortho-C*, J_{C-P} = 12.1 Hz), 126.05 (*ortho-C*, J_{C-P} = 12.0 Hz), 57.75, 56.68, 55.0 (N−*C*H_2), 43.1, (P−*C*H, J_{C-P} = 62.9 Hz), 35.7 (*C*Me_3), 34.4 (*C*H_2CO), 31.9 (C*Me*$_3$), 29.9, 29.1, 27.6, 27.3 (*C*HMe_2), 21.4, 21.2, 21.1, 20.8 (CH*Me*$_2$). ^1H (ppm, $CDCl_3$): 7.98−7.43 (m, Ar), 4.40−4.35 (P−*H*, m), 3.48−2.40 (m), 2.05−1.70 (C*H*Me_2), 1.30−0.7 (m, Me).

X-ray Analysis of B. A colorless blocklike crystal of approximate dimensions 0.32 × 0.26 × 0.22 mm was mounted on a

(46) Hartman, J. R.; Combariza, M. Y.; Vachet, R. W. *Inorg. Chim. Acta* **2004**, *357*, 51−58.
(47) Combariza, M. Y.; Vachet, R. W. *J. Phys. Chem. A* **2004**, *108*, 1757−1763.
(48) Combariza, M. Y.; Fermann, J. T.; Vachet, R. W. *Inorg. Chem.* **2004**, *43*, 2745−2753.
(49) Combariza, M. Y.; Vachet, R. W. *J. Am. Soc. Mass Spectrom.* **2004**, *15*, 1128−1135.
(50) Lim, J.; Vachet, R. W. *Anal. Chem.* **2004**, *76*, 3498−3504.
(51) Bridgewater, J. D.; Vachet, R. *J. Am. Soc. Mass Spectrom.* **2005**, *341*, 122−130.
(52) Gresham, G. L.; Gianotto, A. K.; de Harrington, P.; Cao, L.; Scott, J. R.; Olson, J. E.; Appelhans, A. D.; Van Stipdonk, M. J.; Groenewold, G. S. *J. Phys. Chem. A* **2003**, *107*, 8530−8538.
(53) Goenewold, G. S.; Van Stipdonk, M. J.; Gresham, G. L.; Chien, W.; Bulleigh, K.; Howard, A. *J. Mass Spectrom.* **2004**, *39*, 752−761.
(54) Van Stipdonk, M. J.; Chien, W.; Anbalagan, V.; Gresham, G. L.; Groenewold, G. S. *Int. J. Mass Spectrom.* **2004**, *237*, 175−183.
(55) Chien, W.; Anbalagan, V.; Zandler, M.; Van Stipdonk, M.; Hanna, D.; Gresham, G.; Groenewold, G. *J. Am. Soc. Mass Spectrom.* **2004**, *15*, 777−783.
(56) Van Stipdonk, M. J.; Chien, W.; Anbalagan, V.; Bulleigh, K.; Hanna, D.; Groenewold, G. S. *J. Phys. Chem. A* **2004**, *108*, 10448−10457.
(57) Anbalagan, V.; Chien, W.; Gresham, G. L.; Groenewold, G. S.; Van Stipdonk, M. J. *Rapid Commun. Mass Spectrom.* **2004**, *18*, 3028−3034.
(58) Platt, A. W. G.; Fawcett, J.; Hughes, R. S.; Russell, D. R. *Inorg. Chim. Acta* **1999**, *295*, 146−152.
(59) Stewart, I. I.; Horlick, G. *Anal. Chem.* **1994**, *66*, 3983−3993.
(60) Curtis, J. M.; Derrick, P. J.; Schnell, A.; Constantin, E.; Gallagher, R. T.; Chapman, J. R. *Inorg. Chim. Acta* **1992**, *201*, 197−201.
(61) Colton, R.; Klaui, W. *Inorg. Chim. Acta* **1993**, *211*, 235−242.
(62) Jackson, G. P.; Gibson, J. K.; Duckworth, D. C. *Int. J. Mass Spectrom.* **2002**, *220*, 419−441.
(63) Beer, P. D.; Brindley, G. D.; Fox, O. D.; Grieve, A.; Ogden, M. I.; Szemes, F.; Drew, M. G. B. *J. Chem. Soc., Dalton Trans.* **2002**, 3101−3111.
(64) Lees, A. M. J.; Charnock, J. M.; Kresinski, R. A.; Platt, A. W. G. *Inorg. Chim. Acta* **2001**, *312*, 170−182.
(65) Chapon, D.; Husson, C.; Delangle, P.; Lebrun, C.; Vottero, P. J. A. *J. Alloys Compd.* **2001**, *323*, 128−132.
(66) Evans, W. J.; Johnston, M. A.; Fujimoto, C. H.; Greaves, J. *Organometallics* **2000**, *19*, 4258−4265.
(67) Zhang, J. J.; Zhang, W.; Luo, Q. H.; Mei, Y. H. *Polyhedron* **1999**, *18*, 3637−3642.
(68) Marcalo, J.; deMatos, A. P.; Evans, W. J. *Organometallics* **1997**, *16*, 3845−3850.
(69) Colette, S.; Amekraz, B.; Madic, C.; Berthon, L.; Cote, G.; Moulin, C. *Inorg. Chem.* **2002**, *41*, 7031−7041.
(70) Colette, S.; Amekraz, B.; Madic, C.; Berthon, L.; Cote, G.; Moulin, C. *Inorg. Chem.* **2003**, *42*, 2215−2226.
(71) Lau, R. L. C.; Jiang, J. Z.; Ng, D. K. P.; Chan, T. W. D. *J. Am. Soc. Mass Spectrom.* **1997**, *8*, 161−169.
(72) Groenewold, G. S.; Van Stipdonk, M. J.; Gresham, G. L.; Chien, W.; Bulleigh, K.; Howard, A. *J. Mass Spectrom.* **2004**, *39*, 752−761.
(73) Hutschka, F.; Dedieu, A.; Troxler, L.; Wipff, G. *J. Phys. Chem. A* **1998**, *102*, 3773−3781.
(74) Troxler, L.; Dedieu, A.; Hutschka, F.; Wipff, G. *J. Mol. Struct. THEOCHEM.* **1998**, *431*, 151−163.
(75) Guillory, P.; Kapoor, R. N.; Pannell, K. H.; Schulte, L.; McKee, S. D.; Zhang, Z. Y.; Bartsch, R. C. *Synth. Commun.* **2003**, *33*, 325−330.

Table 1. Crystal Data and Structure Refinement for Compound **B**

empirical formula	$C_{40}H_{65}N_2O_3P$
fw	652.91
T	123(2)
radiation and wavelength	Mo Kα, $\lambda = 0.71073$ Å
cryst syst	triclinic
space group	$P\bar{1}$
unit cell dimensions	$a = 13.251(2)$ Å
	$b = 13.426(2)$ Å
	$c = 13.845(2)$ Å
	$\alpha = 104.155(3)°$
	$\beta = 112.198(3)°$
	$\gamma = 107.304(3)°$
V	1992.1(6) Å^3
Z	2
D (calcd)	1.088 Mg/m^3
abs coeff, μ	0.105 mm^{-1}
F(000)	716
cryst size	0.32 × 0.26 × 0.22 mm
max and min transm	0.9772 and 0.9671
θ-range for data collection	$1.74° \le \theta \le 28.42°$
index ranges	$-16 \le h \le 17$; $-17 \le k \le 17$; $-18 \le l \le 18$
reflns collected	23236
reflns $I > 2\sigma(I)$	6116
final R indices [$I > 2\sigma(I)$]	R1 = 0.0688, wR2 = 0.1433
R indices (all data)	R1 = 0.0864, wR2 = 0.1514

nylon loop and used for crystallographic analysis. The X-ray intensity data were measured at 123(2) K on a Bruker SMART APEX CCD area detector system equipped with a graphite monochromator and a Mo Kα fine-focus sealed tube ($\lambda = 0.71073$ Å). The detector was placed 5.968 cm from the crystal.

A total of 2400 frames were collected with a scan width of 0.3° in ω and an exposure time of 10 s/frame. The frames were integrated with the Bruker SAINT software package using a narrow-frame integration algorithm yielding the unit cell parameters reported in Table 1. Data were corrected for absorption effects using the multiscan technique (SADABS) and used for structure solution and refinement with the Bruker SHELXTL software package. The final anisotropic full-matrix least-squares refinement on F^2 converged at R1 = 6.88% for the observed data and at wR2 = 15.14% for all data with a GOF of 1.160. A complete summary of collection and refinement data are given in Table 1, the structure is illustrated in Figure 2 , and selected bond lengths and angles are presented in Table 2.

Instrumentation. All mass spectrometry experiments were performed using 99% methanol/1% nitric acid solutions, 5.0×10^{-5} M in lanthanide ions and 5.0×10^{-6} M in ligands, on a Finnigan LCQ-Duo ion trap mass spectrometer using the Xcalibur (Finnigan, San Jose, CA) software package and an electrospray ionization source. The ion trap was operated at a base pressure of nominally 5×10^{-6} Torr with helium. For ESI experiments, the sample flow rate was 3 μL/min, and upon sample introduction, the pressure in the analyzer region increased to 1×10^{-5} Torr. The electrospray voltage used was 4.5 kV, and the heated capillary was set to 180 °C. Ionization and trapping conditions were optimized for maximum intensity of the $[2\cdot\mathbf{A} + La(NO_3)_2]^+$ ion (m/z 1229) and were kept constant throughout.

Results and Discussion

Ligand Synthesis and Characterization. The synthesis of ligand **A** was recently reported[75] as was its structure, along with those of the uranyl and some organotin chloride complexes.[76] The presence of the potentially reactive P(O)−CH_2−C(O) methylene group suggests that a series of derivatives could be forthcoming via substitutions at this

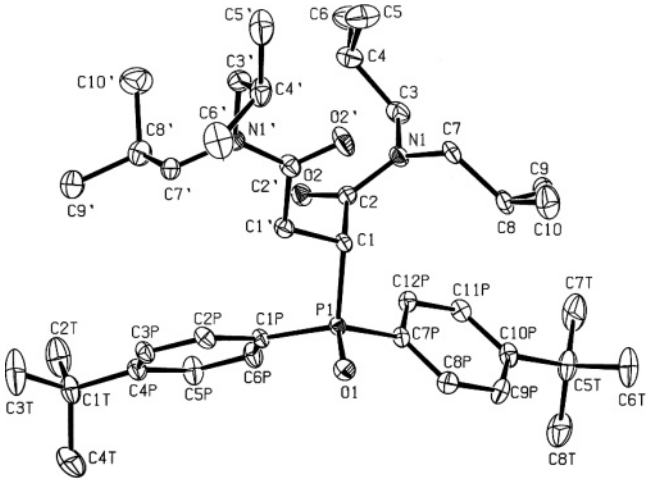

Figure 2. Structure of tridentate CMPO ligand (t-BuC_6H_4)$_2$P(O)CH[CH_2C(O)N(i-Bu)$_2$]C(O)N(i-Bu)$_2$ (**B**).

Table 2. Selected Bond Lengths (Å) and Angles (deg) for Compound **B**

P1−O1	1.485(2)	P1−C7P	1.805(2)
P1−C1P	1.806(2)	P1−C1	1.843(2)
O2−C2	1.236(2)	O2′−C2′	1.228(3)
N1−C2	1.350(3)	N1−C3	1.466(3)
N1−C7	1.473(3)	N1′−C2′	1.349(3)
N1′−C7′	1.470(3)	N1′−C3′	1.470(3)
O1−P1−C7P	112.42(9)	O1−P1−C1P	111.00(9)
C7P−P1−C1P	108.43(9)	O1−P1−C1	108.31(9)
C7P−P1−C1	106.68(9)	C1P−P1−C1	109.89(9)
C2−N1−C3	116.5(2)	C2−N1−C7	123.8(2)
C3−N1−C7	119.6(2)	C2′−N1′−C7′	123.7(2)
C2′−N1′−C3′	117.4(2)	C7′−N1′−C3′	118.9(2)

position. Indeed, the Paine group reported that treatment of $R_2P(O)CH_2C(O)NEt_2$ (R = EtO, Ph) with NaH followed by addition of substituted benzyl chlorides[77] and *N*,*N*-diethylchloroacetamide[78] resulted in the formation of $R_2P(O)CHR'C(O)NEt_2$ (R′ = CH_2Ar and CH_2CONEt_2, respectively). Thus, similar treatment of **A** with powdered NaH followed by addition of $ClCH_2C(O)N(iBu_2)$ resulted in the formation of the tridentate ligand **B** (eq 1). The formation of **B** presents

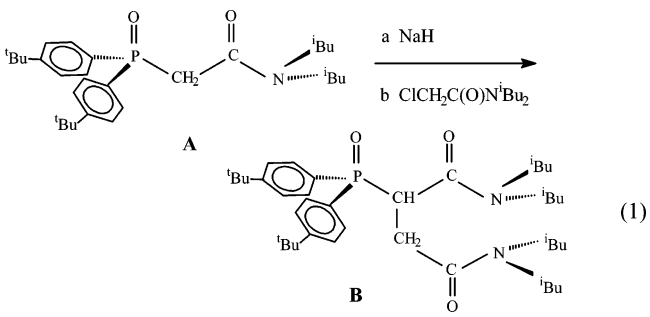

(1)

an opportunity to investigate the efficacy of increasing the multidentate character of CMPO ligands.

All NMR and IR spectroscopic data of **B** are in accord with the proposed structure and in keeping with related

(76) Kapoor, R. N.; Guillory, P.; Schulte, L.; Cervantes-Lee, F.; Haiduc, I.; Parkanyi, L.; Pannell, K. H. *Appl. Organomet. Chem.* **2005**, *19*, 510−517.
(77) Conary, G. S.; Meline, R. L.; Caudle, L. J.; Duesler, E. N.; Paine, R. T. *Inorg. Chim. Acta* **1991**, *189*, 59−66.
(78) McCabe, D. J.; Bowen, S. M.; Paine, R. T. *Synthesis* **1986**, 319.

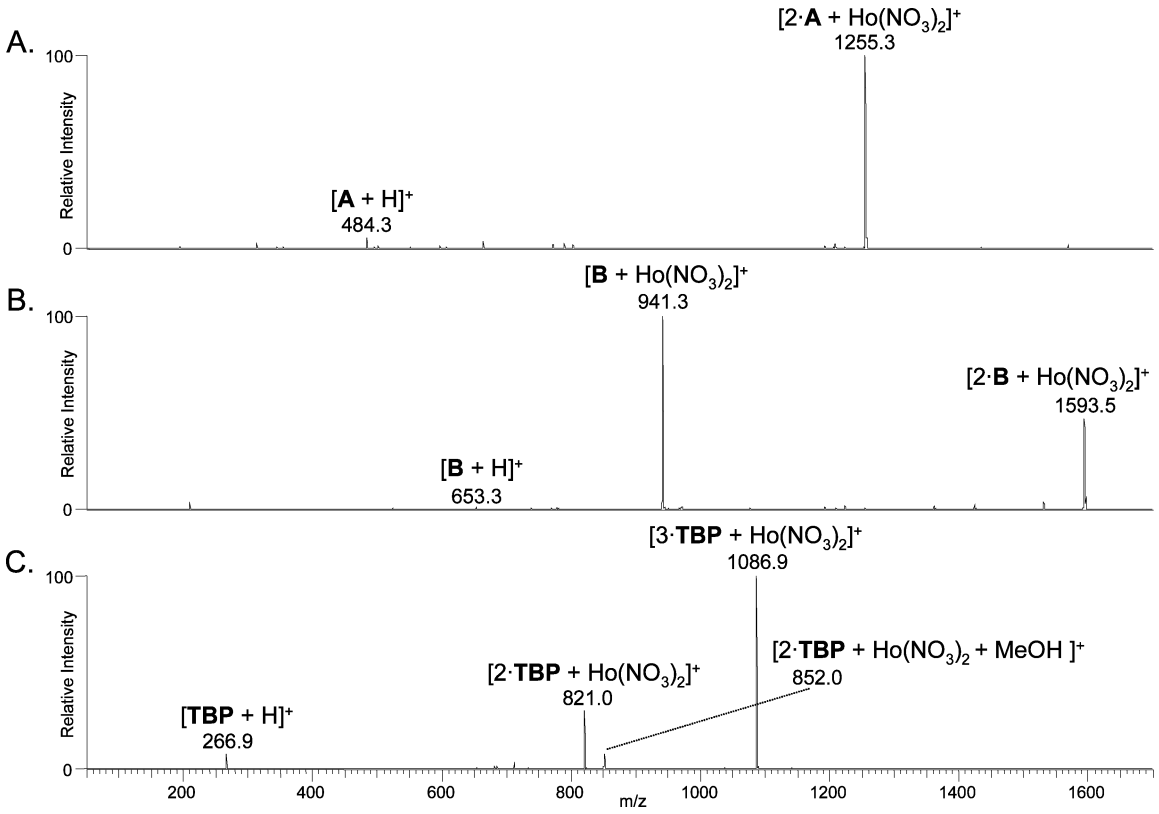

Figure 3. ESI mass spectra of (A) ligand **A**, (B) ligand **B**, and (C) tributyl phosphate with $HoCl_3$ in 99:1 methanol/HNO_3.

ligands.[75−78] Because of the asymmetric center at the P*C*H atom, many of the NMR signals are doubled, as noted above. For example, the *ipso*-aryl carbons are noted as a pair of doublets ($^1J_{C-P}$ = 100.9 Hz) and the chemical shift between the two sets diminishes progressively with the distance of the C atom to the P*C*H atom such that the *para*-aryl carbon atom appears as a single doublet ($^4J_{C-P}$ = 2.56 Hz). Similarly, the N*C*H_2 and *C*HMe_2 atoms of both acetamides appear as a doubled set of two singlets because of the well-established nature of the cis/trans orientation of acetamide alkyl substituents on N. However, interestingly, for the two distinct acetamide groups, one set of methyl groups shows up as a doubled set of two singlets, and the other set exhibits a single resonance. This latter situation is also noted for the unsubstituted CMPO precursor and *N*,*N*-diisobutylchloroacetamide.

We were able to obtain crystals of **B** suitable for X-ray analysis, and the structure is illustrated in Figure 2. In general, there are no surprises concerning the various bond lengths and angles (Table 2). The P═O bond length of **B** at 1.458(2) Å is somewhat shorter than that of the parent CMPO ligand **A**, 1.481(2) Å, reflecting the electron-withdrawing capacity of the additional carbamoyl grouping. The two C═O bonds with distances of 1.236(2) (PCH*C*(*O*)) and 1.228(3) Å (PCHCH_2*C*(*O*)) indicate the equivalence of the PC*C*(*O*) groups in **A** (1.231(3) Å)[76] and **B**, and the other CO group is somewhat shortened. As expected, the *N*−*C*(O) bonds for both carbamoyl groups, 1.350(3) and 1.349(3) Å, are significantly shorter than the *N*−*C*H_2 bonds (1.466(3)−1.473(3) Å) because of the (C−O^-)═N^+ resonance contribution to the amide linkage. Furthermore, the trigonal planar arrangement at the N atoms (sum of the bond angles at N = 359.9(2)° and 360.0(2)°) is a further illustration of this bonding arrangement.

An interesting feature of the conformation of the ligand **B** is that the two independent C═O groups, C2′═O2 and C2′═O2′, align themselves to take advantage of the intramolecular dipolar $C^{\delta+}-O^{\delta-}$ stabilizing interaction. Thus, the C2═O2′ and C2′═O2 internuclear distances are 3.22 and 3.66 Å, close to the sum of the van der Waals radii, 3.25 Å. The actual energy of such an interaction is low. For example, experimental results on the dimerization of acetone resulted in ∼2 kcal/mol stabilization energy compared to that of two noninteracting molecules.[79] In the present case, modeling the two amide groups as dimethylacetamide, a $Me_2NC(O)CH_3$ dimer resulted in a stabilization of ∼2.3−3.3 kcal/mol with inter C and O distances similar to those reported above.[80] Such an interaction is clearly sufficient to direct the crystallization process to incorporate such a dipole alignment. Although this confirmation is not one that would facilitate tridentate binding to a metal center, complexes of this ligand are currently under investigation and any conformational change needed for such binding is not great.

Stoichiometries of Complexes Detected by ESI-MS. Analysis of solutions containing a 10:1 concentration ratio of metal/ligand in 100% methanol by ESI-MS produced

(79) Park, S. M.; Herndon, W. C. *Tetrahedron Lett.* **1978**, 2363−2366.
(80) The calculations were kindly performed by Professor W. C. Herndon using both a DFT/B3LYP/6-31G** (2.343 kcal/mol) and an HF 6-31G** (3.33 kcal/mol) level of theory. The latter approach is known to give a smaller error in the basis set superposition problem, thus, the overall stabilizing effect of the dipole−dipole alignment is not in doubt.

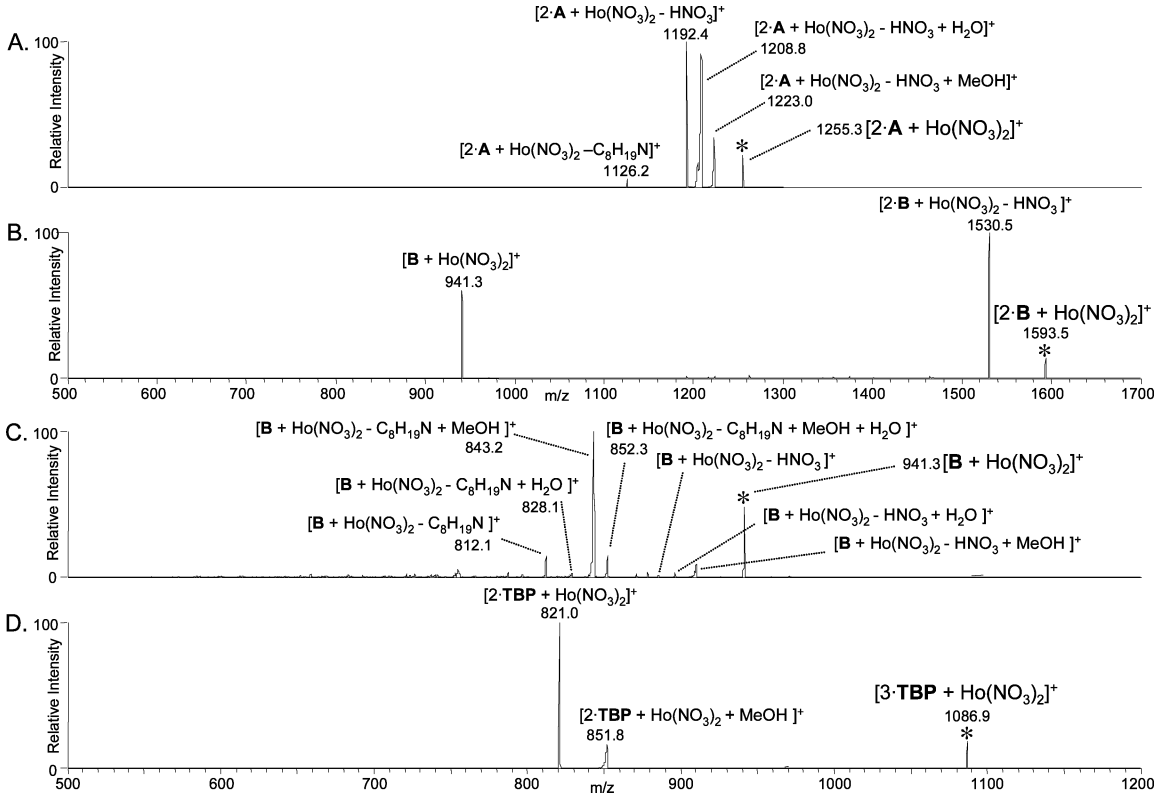

Figure 4. CAD mass spectra of (A) $[2\cdot\mathbf{A} + Ho(NO_3)_2]^+$, (B) $[2\cdot\mathbf{B} + Ho(NO_3)_2]^+$, (C) $[\mathbf{B} + Ho(NO_3)_2]^+$, and (D) $[3\cdot TBP + Ho(NO_3)_2]^+$. The precursor ions are indicated by asterisks.

spectra that were difficult to interpret because of the number of different ionic species observed. To obtain less complex, more reproducible results, it was determined that the addition of 1% nitric acid to methanolic solutions containing lanthanide ion/ligand concentrations of $5.0 \times 10^{-5}/5.0 \times 10^{-6}$ M resulted in the observation of ions containing solely nitrate counteranions and allowed the type of metal ligand complexes formed to be readily evaluated. Because of the superiority of these data, the same solution composition was used for all of the studies reported herein. Holmium was chosen as the representative lanthanide ion because it is monoisotopic. Figure 3 shows that under these conditions the spectra are simplified, with dominant ions due to $[n\cdot L + Ho(NO_3)_2]^+$ complexes.

In the case of the bidentate ligand **A**, the only ion with significant abundance appears at *m*/*z* 1255, which represents the $[2\cdot\mathbf{A} + Ho(NO_3)_2]^+$ complex (Figure 3A). Protonated **A** is also observed (*m*/*z* 484) at ~5% relative abundance. Under these experimental conditions, **A** strongly favors the formation of the 2:1:2 (ligand/metal/anion) complex.

The potentially tridentate CMPO ligand, **B**, was analyzed under the same conditions (Figure 3B). Unlike **A**, the most abundant ion (*m*/*z* 941) represents the 1:1:2 ligand/metal/anion complex, $[\mathbf{B} + Ho(NO_3)_2]^+$, with the 2:1:2 complex ($[2\cdot\mathbf{B} + Ho(NO_3)_2]^+$, *m*/*z* 1593) present at ~50% relative abundance. Both the lower abundance of the $[2\cdot\mathbf{B} + Ho(NO_3)_2]^+$ complex and the presence of the abundant singly ligated complex, $[\mathbf{B} + Ho(NO_3)_2]^+$ (which is not observed with **A**), can be attributed to the extra coordination site of **B** because of the additional *N*,*N*-diisobutylacetamide substituent which allows complete coordination of the metal ion by a single ligand. The extra carbamoyl substituent on **B** may also cause some steric hindrance to limit formation of the $[2\cdot\mathbf{B} + Ho(NO_3)_2]^+$ complex.

The monodentate tributyl phosphate was also analyzed in the presence of holmium chloride under the same solution conditions, producing abundant $[2\cdot TBP + Ho(NO_3)_2]^+$ and $[3\cdot TBP + Ho(NO_3)_2]^+$ species. The tributyl phosphate ligand is smaller than either **A** or **B**, so three monodentate ligands are able to arrange themselves in a stable complex around a single metal ion without the steric constraints of **A** and **B**.

Tandem Mass Spectrometry of Lanthanide/Ligand Complexes. Further information about the relative stabilities of the lanthanide/ligand complexes in the gas phase can be obtained from collisionally activated dissociation experiments. Dissociation of the $[2\cdot\mathbf{A} + Ho(NO_3)_2]^+$ complex (Figure 4A) provides evidence for strong ligand−metal interactions between each of the bound ligands and holmium. Upon activation, this complex does not dissociate via the loss of either of the bound CMPO ligands but rather by the loss of nitric acid (−63 amu, resulting in an ion of *m*/*z* 1192) or by the loss of a diisobutylamine substituent (129 amu, resulting in an ion of *m*/*z* 1126). The product ion at the *m*/*z* of 1192 from the loss of HNO_3 undergoes rapid, spontaneous addition of water or methanol, as verified by MS^n experiments (data not shown), producing the unusually broad adduct peaks at *m*/*z* of 1209 and 1223 in Figure 4A. These adducts are interesting because they suggest that upon removal of a nitric acid molecule, i.e., the coordinating nitrate ion, the holmium ion becomes insufficiently solvated and therefore picks up a molecule of adventitious water or methanol in the ion trap. This dissociation/association

Scheme 1

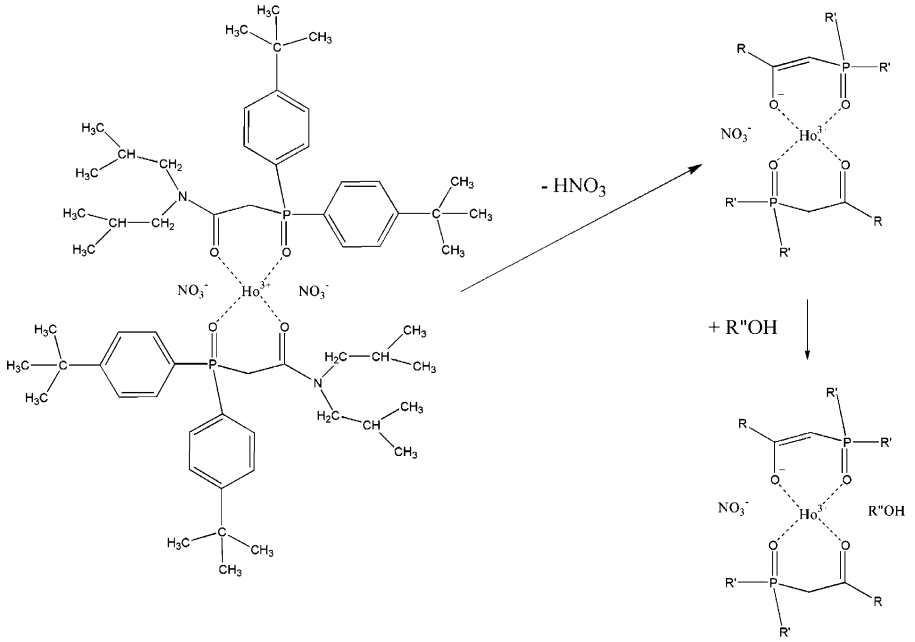

reaction is depicted in Scheme 1. The two ions that result from solvent adduction (nominally $m/z = 1209$ and 1223) have apparent m/z values that are 1−2 amu lower than would be expected on the basis of their chemical formulas. Also, the peaks are broader than normal and have non-Gaussian shapes with low m/z tails. These features are characteristic of weakly bound solvent adducts in a quadrupole ion trap.[81]

Ligand **B** produces two abundant complexes: $[2\cdot\mathbf{B} + Ho(NO_3)_2]^+$ and $[\mathbf{B} + Ho(NO_3)_2]^+$. Collisional activation of the $[2\cdot\mathbf{B} + Ho(NO_3)_2]^+$ complex results in two distinct dissociation pathways (Figure 4B). The first is the loss of nitric acid from the precursor complex (resulting in a m/z of 1531), as was seen for the analogous $[2\cdot\mathbf{A} + Ho(NO_3)_2]^+$ complex. This product, however, does not react with adventitious solvent molecules to form other secondary adduct species. The other major fragment ion ($m/z = 941$) involves the loss of an entire CMPO ligand. The fact that the $[2\cdot\mathbf{B} + Ho(NO_3)_2]^+$ complex loses an intact ligand, whereas the analogous complex for **A** does not, suggests both that the second ligand is more weakly bound than the first and that the first ligand can function as a polydentate ligand that effectively solvates the lanthanide ion.

Dissociation of the other complex, $[\mathbf{B} + Ho(NO_3)_2]^+$ (Figure 4c), results in behavior that is somewhat similar to that observed for the $[2\cdot\mathbf{A} + Ho(NO_3)_2]^+$ complex. The first fragmentation route involves the loss of a diisobutylamine portion of the ligand (giving m/z 812), which may be followed by rapid, spontaneous solvent adduction, leading to the secondary products at m/z of 829, 843, and 857 via addition of water, methanol, or water and methanol, respectively. The formation of intense adduct peaks following dissociation could suggest that the nitrogen atom in the diisobutylamine portion of the ligand is involved in the coordination of the metal ion in the precursor complex and that removal of this ligand substituent results in insufficient solvation of the metal ion, thus promoting solvent adduction.[41−49] Certainly, the loss of this N group will eliminate the presence of the more basic $-C-(O^-)=N^+R_2$ form of this grouping, thereby increasing the need for further coordination at the metal center. The second dissociation route of $[\mathbf{B} + Ho(NO_3)_2]^+$ is the loss of HNO_3, as was observed for the $[2\cdot\mathbf{A} + Ho(NO_3)_2]^+$ and $[2\cdot\mathbf{B} + Ho(NO_3)_2]^+$ complexes.

Dissociation of the $[3\cdot TBP + Ho(NO_3)_2]^+$ complex (Figure 4d) yields a single dominant fragmentation pathway: the loss of an intact TBP ligand (resulting in a m/z of 821). The loss of one of the ligand molecules leaves the metal ion insufficiently coordinated, resulting in the spontaneous formation of a methanol adduct at a m/z of 852. The formation of this adduct is interesting because it provides further evidence that at least three monodentate tributyl phosphate ligands (as well as two nitrate anions) are necessary to completely solvate the holmium cation in the gas phase.

Table 3. Electrospray Mass Spectral Data of 10:1:1 Mixed Ligand Solutions in 99:1 Methanol/HNO_3

ligands in solution	observed m/z	complex identity	relative abundance (%)
A, TBP	772.3	$[\mathbf{A} + Ho(NO_3)_2]^+$	1
	1038.1	$[\mathbf{A} + TBP + Ho(NO_3)_2]^+$	35
	1086.9	$[3\cdot TBP + Ho(NO_3)_2]^+$	5
	1255.3	$[2\cdot\mathbf{A} + Ho(NO_3)_2]^+$	100
B, TBP	941.3	$[\mathbf{B} + Ho(NO_3)_2]^+$	56
	1086.9	$[3\cdot TBP + Ho(NO_3)_2]^+$	3
	1207.1	$[\mathbf{B} + TBP + Ho(NO_3)_2]^+$	7
	1593.5	$[2\cdot\mathbf{B} + Ho(NO_3)_2]^+$	100
A, **B**	772.3	$[\mathbf{A} + Ho(NO_3)_2]^+$	0.1
	941.3	$[\mathbf{B} + Ho(NO_3)_2]^+$	22
	1255.3	$[2\cdot\mathbf{A} + Ho(NO_3)_2]^+$	63
	1424.3	$[\mathbf{A} + \mathbf{B} + Ho(NO_3)_2]^+$	100
	1593.5	$[2\cdot\mathbf{B} + Ho(NO_3)_2]^+$	37

(81) Wells, J. M.; Plass, W. R.; Patterson, G. E.; Zheng, O. Y.; Badman, E. R.; Cooks, R. G. *Anal. Chem.* **1999**, *71*, 3405−3415.

Table 4. Electrospray Tandem Mass Spectral Data of Mixed Ligand Complexes[a]

precursor complex	precursor *m/z*	fragment *m/z*	process[b]	product identity	relative abundance (%)
$[\mathbf{A} + \text{TBP} + \text{Ho}(\text{NO}_3)_2]^+$	1038.1	831.5	−TBP, +ACN, $+\text{H}_2\text{O}$	$[\mathbf{A} + \text{Ho}(\text{NO}_3)_2 + \text{ACN} + \text{H}_2\text{O}]^+$	6
		812.4	−TBP, +ACN	$[\mathbf{A} + \text{Ho}(\text{NO}_3)_2 + \text{ACN}]^+$	53
		803.3	−TBP, +MeOH	$[\mathbf{A} + \text{Ho}(\text{NO}_3)_2 + \text{MeOH}]^+$	100
		789.0	−TBP, $+\text{H}_2\text{O}$	$[\mathbf{A} + \text{Ho}(\text{NO}_3)_2 + \text{H}_2\text{O}]^+$	24
		772.3	−TBP	$[\mathbf{A} + \text{Ho}(\text{NO}_3)_2]^+$	16
$[\mathbf{B} + \text{TBP} + \text{Ho}(\text{NO}_3)_2]^+$	1207.1	941.3	−TBP	$[\mathbf{B} + \text{Ho}(\text{NO}_3)_2]^+$	100
$[\mathbf{A} + \mathbf{B} + \text{Ho}(\text{NO}_3)_2]^+$	1424.3	1361.5	$-\text{HNO}_3$	$[\mathbf{A} + \mathbf{B} + \text{Ho}(\text{NO}_3)_2 - \text{HNO}_3]^+$	100
		941.3	−A	$[\mathbf{B} + \text{Ho}(\text{NO}_3)_2]^+$	10

[a] ACN is acetonitrile and TBP is tributyl phosphate [b] "Process" indicates the dissociation and possible solvent adduction pathway.

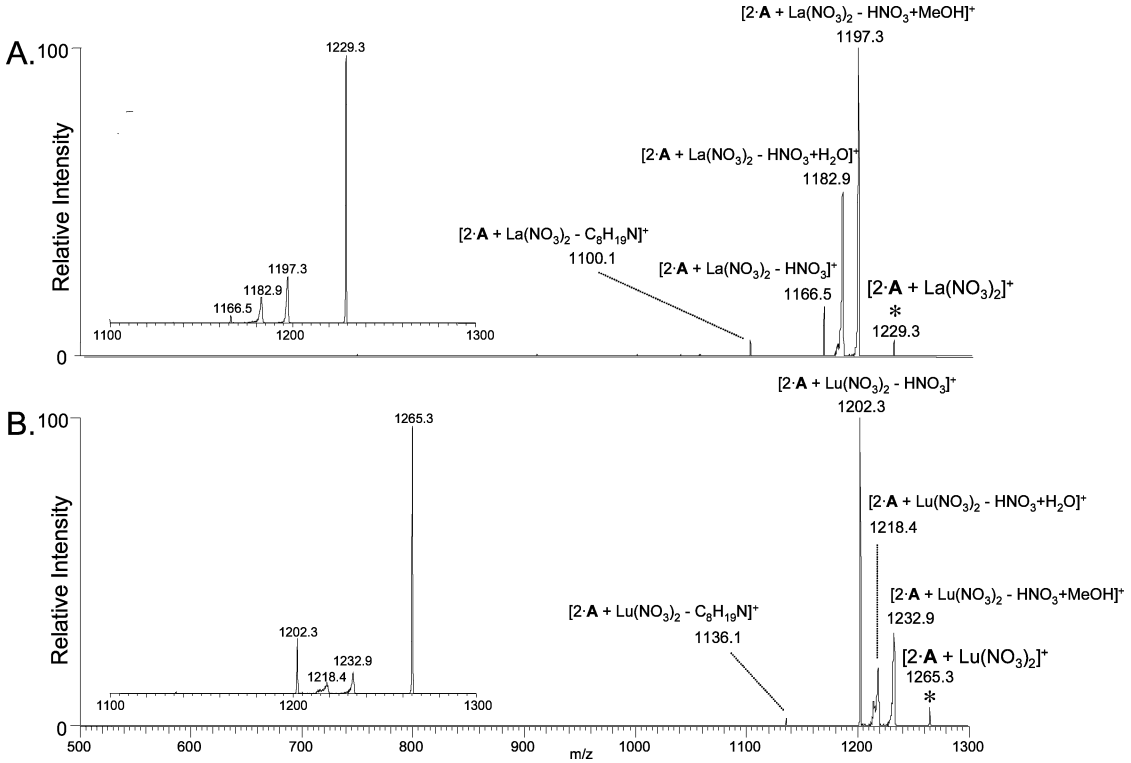

Figure 5. CAD mass spectra (95% fragmentation) of the (A) $[2\cdot\mathbf{A} + \text{La}(\text{NO}_3)_2]^+$, and (B) $[2\cdot\mathbf{A} + \text{Lu}(\text{NO}_3)_2]^+$ complexes. Insets are 50% dissociation CAD spectra (A) at 2.60 V and (B) at 2.34 V. The precursor ions are indicated by asterisks.

The involvement of tributyl phosphate in the PUREX and TRUEX processes[4,6] makes it interesting to probe the intrinsic lanthanide-binding properties of tributyl phosphate relative to those of the CMPO ligands. Thus, solutions containing two of the ligands (**A** or **B** and TBP) and HoCl_3 were analyzed by ESI-MS and the resulting heteroligand complexes were subjected to CAD. ESI of solutions containing each of the ligand combinations resulted in the formation of the expected homoligand complexes (see Table 3) as well as the formation of relatively low-abundance heteroligand complexes containing $\text{Ho}(\text{NO}_3)_2$ and either TBP and **A** or TBP and **B**. Upon CAD, the loss of tributyl phosphate was the dominant fragmentation pathway regardless of the identity of the CMPO ligand (see Table 4). This suggests that the interaction of TBP with holmium in each of these complexes is less energetically favorable than the CMPO/holmium interaction, which is an expected result when mono- and multidentate ligands are compared.

In addition, the MS/MS data allow comparison of the relative stabilities of the complexes in the gas phase based on the energy required to remove tributyl phosphate from each of the complexes and dissociate 50% (an arbitrary quantity) of the parent complexes. After correction for degrees of freedom to account for the different number of vibrational modes in each complex,[82] a significantly greater CAD voltage is required for a comparable extent of dissociation of the $[\mathbf{A} + \text{TBP} + \text{Ho}(\text{NO}_3)_2]^+$ complex (2.93 V) relative to that of the $[\mathbf{B} + \text{TBP} + \text{Ho}(\text{NO}_3)_2]^+$ complex (1.77 V), indicating that the tributyl phosphate ligand is more strongly bound to holmium in the $[\mathbf{A} + \text{TBP} + \text{Ho}(\text{NO}_3)_2]^+$ complex than in the $[\mathbf{B} + \text{TBP} + \text{Ho}(\text{NO}_3)_2]^+$ complex as a direct result of the tridentate capacity of **B**.

A solution containing both of the CMPO ligands was also analyzed. The heteroligand complex corresponding to $[\mathbf{A} + \mathbf{B} + \text{Ho}(\text{NO}_3)_2]^+$ was detected at a *m/z* of 1424 (Table 3). Upon collisional activation, this heteroligand complex dissociated by two dominant fragment pathways (Table 4): the loss of nitric acid and the loss of **A**. The dominance of the

(82) Jones, J. L.; Dongre, A. R.; Somogyi, A.; Wysocki, V. H. *J. Am. Chem. Soc.* **1994**, *116*, 8368−8369.

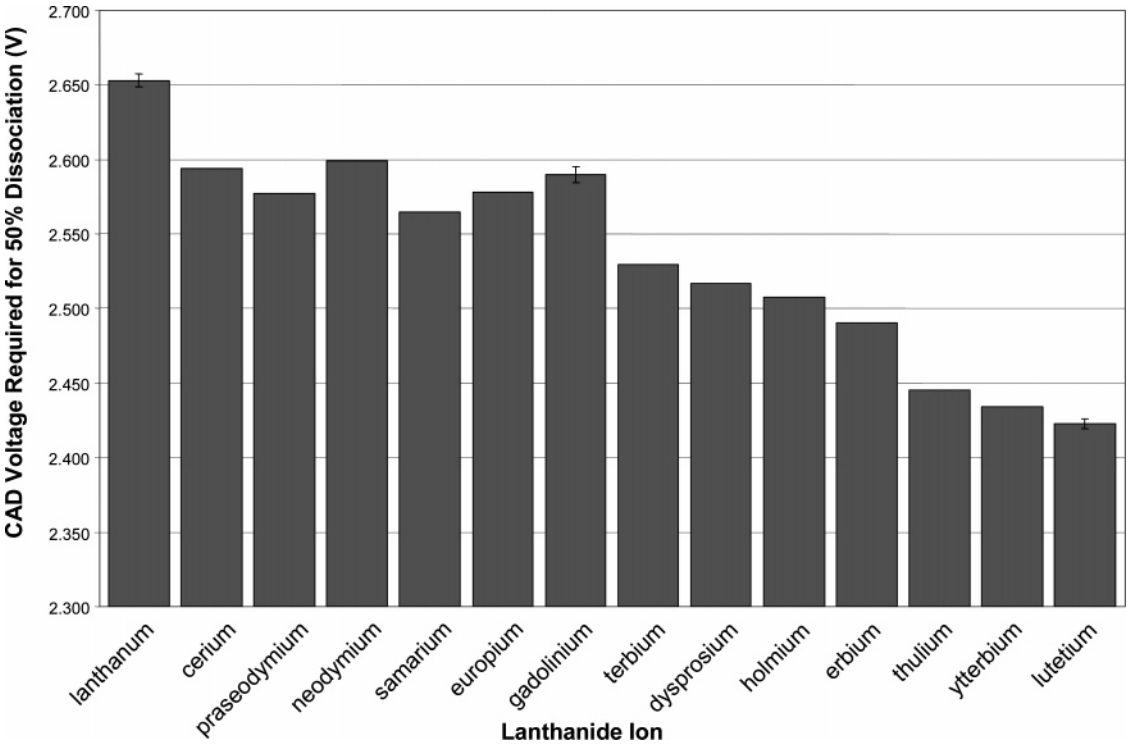

Figure 6. CAD voltages required for 50% dissociation of $[2{\cdot}\mathbf{A} + Ln(NO_3)_2]^+$ complexes.

first dissociation pathway, the loss of nitric acid instead of the loss of either ligand, confirms the intrinsic stability of this complex. The lack of solvent adducts formed upon the loss of nitric acid suggests that the combination of these two ligands more effectively solvates the lanthanide ion than do two molecules of **A**.

Metal-Dependent Dissociation Trends. Collisionally activated dissociation was also used to probe the metal-dependent trends in the fragmentation behavior of the complexes containing **A** or **B**. Such trends are evident by examination of the threshold dissociation energies and the relative efficiencies of the solvent coordination process. An example of the differences in dissociation behavior for the $[2{\cdot}\mathbf{A} + M(NO_3)_2]^+$ complexes, M = La and Lu, is shown in Figure 5. The primary dissociation pathway for both of the complexes is the elimination of HNO_3, which may be followed by spontaneous solvent coordination of either water or methanol. The extent of the solvent adduction varies substantially for the two complexes, with far more occurring for the lanthanum complexes than for the lutetium complexes. These adducts arise because the product formed via the loss of nitric acid is sufficiently unstable and reactive such that subsequent solvent attachment stabilizes the complex. The greater extent of solvent addition to the La^{3+} ion presumably reflects the weaker coordination of the larger metal ion by the CMPO ligand, a phenomenon that is associated with its lower electrostatic potential (q/r).

Second, the collisional energy needed to achieve the same extent of dissociation (i.e., such that 50% of the precursor ions are converted to fragment ions) is significantly different for the two complexes. Greater collision voltages are required to dissociate more stable metal−ligand interactions. A collision voltage of 2.60 V is needed for the $[2{\cdot}\mathbf{A} + La(NO_3)_2]^+$ complex as compared with 2.34 V needed for 50% dissociation of the $[2{\cdot}\mathbf{A} + Lu(NO_3)_2]^+$ complex. Less energy is required to cleave HNO_3 from the corresponding lutetium complex because the two CMPO ligands more strongly coordinate the smaller lutetium ion ($r_{Lu^{3+}} = 1.00$ Å cf. with $r_{La^{3+}} = 1.17$ Å) thereby labilizing the nitrate ligand.[83]

For the complete lanthanide series, the trend in the collision voltages needed to dissociate the complexes are examined and are summarized in Figure 6. For each of the $[2{\cdot}\mathbf{A} + Ln(NO_3)_2]^+$ complexes, the dominant dissociation route is the loss of HNO_3 with subsequent solvent adduction and the collision voltage decreases steadily across the series of lanthanides. A similar trend was observed by the Colette group for DATP (lanthanide complexes based on energy-resolved dissociation in a triple quadrupole mass analyzer).[70]

Equivalent studies on the tridentate ligand **B** produce a similar trend when the dissociation thresholds of the $[2{\cdot}\mathbf{B} + Ln(NO_3)_2]^+$ complexes are compared for each of the lanthanides. In this case, there are two dissociation pathways available: the loss of nitric acid and the loss of an entire **B** ligand. A single multidentate ligand **B** forms more stable complexes with $Ln(NO_3)_2^+$ as the size of the lanthanide ion decreases. In contrast, energy-variable dissociation of the $[3{\cdot}TBP + Ln(NO_3)_2]^+$ complexes does not convey any significant trend across the lanthanide series. This is a counterintuitive result. The expected increase in steric interactions between bound ligands with a decrease in the metal radii and the general increase in electrostatic potential of the Ln^{3+} ions seem to have no systematic effect on the dissociation of tributyl phosphate from the lanthanide complexes.

(83) Cotton, F. A.; Wilkinson, G.; Murillo, C. A.; Bochmann, M. *Advanced Inorganic Chemistry*, 6th ed.; John Wiley & Sons: New York, 1999.

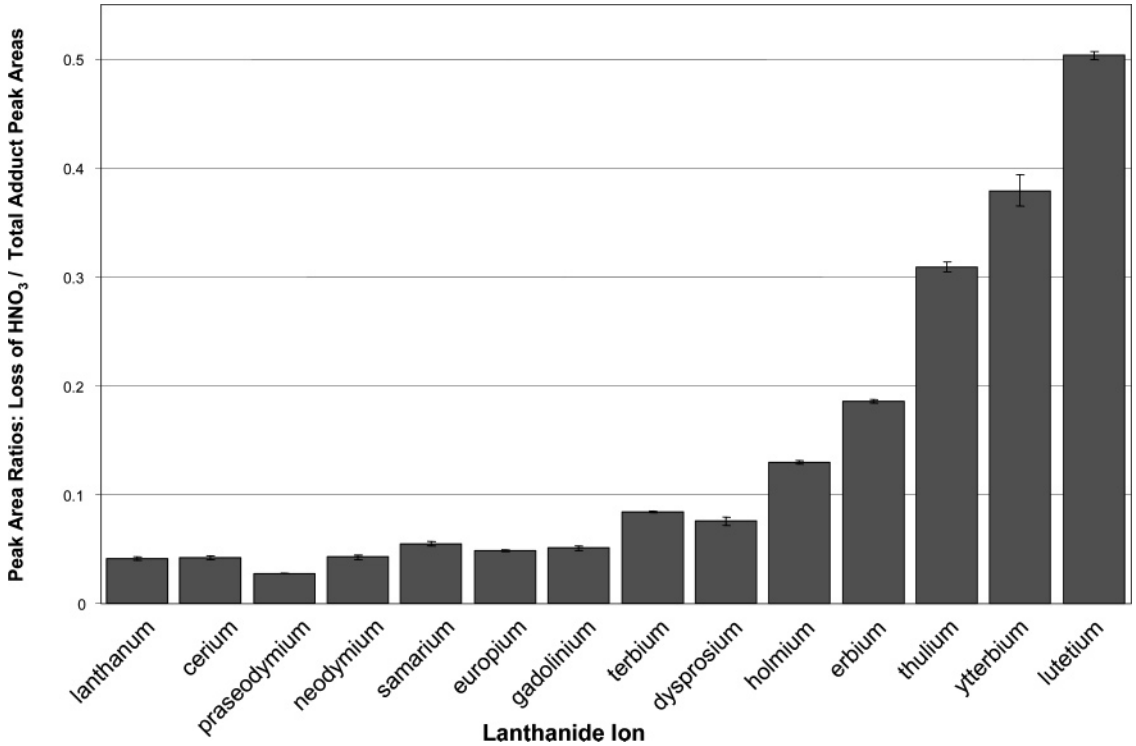

Figure 7. Extent of solvent adduction to fragment ions upon CAD of $[2\cdot\mathbf{A} + Ln(NO_3)_2]^+$ complexes: ratios of peak area for loss of HNO_3 from parent complex/peak areas for all subsequent solvent adducts.

The ratios of the areas of the peaks due to the loss of nitric acid upon CAD of the $[2\cdot\mathbf{B} + Ln(NO_3)_2]^+$ complexes to the sum of the areas of the spontaneous solvent addition peaks are compared for each of the lanthanide complexes at the 50% dissociation level (Figure 7). The ratios increase across the lanthanide series, indicating that solvent adduction becomes less prevalent as the size of the metal ion decreases, paralleling the data shown in Figure 6. Clearly, as the size of the lanthanide ion decreases, the CMPO ligands more efficiently solvate the metal, resulting in more facile cleavage of HNO_3 and lower probability of subsequent solvent addition.

Conclusions

ESI-MS of nitric acid solutions containing the CMPO ligands $(t\text{-}BuC_6H_4)_2P(O)CH_2C(O)N(i\text{-}Bu)_2$ (**A**), $(t\text{-}BuC_6H_4)_2P(O)CH[CH_2C(O)N(i\text{-}Bu)_2]C(O)N(i\text{-}Bu)_2$ (**B**), and tributyl phosphate with dissolved rare-earth salts allowed determination of the favorable gas-phase stoichiometries of lanthanide complexes with each ligand. It was found that ligand **A** most favorably forms $[2\cdot\mathbf{A} + M(NO_3)_2]^+$ complexes, ligand **B** favors formation of $[1\cdot\mathbf{B} + M(NO_3)_2]^+$ complexes, and tributyl phosphate favors formation of $[3\cdot TBP + M(NO_3)_2]^+$ complexes. These results parallel the bidentate, tridentate, and monodentate capacity of the three ligands **A**, **B**, and TBP, respectively.

Tandem mass spectrometry of the $[2\cdot\mathbf{A} + Ho(NO_3)_2]^+$ and $[2\cdot\mathbf{B} + Ho(NO_3)_2]^+$ complexes provided results indicating that the ligand **A** complex requires both ligands for complete solvation of the metal ion, whereas a single ligand **B** (along with two nitrates) is able to effectively solvate the metal ion. Removal of a ligand **A** molecule from the $[2\cdot\mathbf{A} + Ho(NO_3)_2]^+$ complex results in an insufficiently solvated metal ion, evidenced by the spontaneous adduction of solvent molecules to the $[\mathbf{A} + Ho(NO_3)_2]^+$ product ion. In contrast, removal of a single ligand from the $[2\cdot\mathbf{B} + Ho(NO_3)_2]^+$ complex produces the $[\mathbf{B} + Ho(NO_3)_2]^+$ product ion which does not react with solvent molecules, illustrating its relative stability compared to that of the analogous ligand **A** product ion.

Threshold collisionally activated dissociation experiments allowed investigation of the relative stabilities of the $[2\cdot\mathbf{A} + Ln(NO_3)_2]^+$ and the $[2\cdot\mathbf{B} + Ln(NO_3)_2]^+$ complexes formed with different lanthanide ions, both by the energy required for 50% dissociation and by the extent of post-dissociation solvent adduction. Both the collisional energy required for the removal of an HNO_3 molecule from the complex and the extent of subsequent solvent adduction decreases as the ionic radius of the metal ion decreases. These results suggest that the carbamoylmethylphosphine ligands more effectively solvate the smaller, more charge dense lanthanide ions.

Acknowledgment. Funding from the Welch Foundation [grants F-1155 (J.S.B.) and AH-546 (K.H.P.)] is gratefully acknowledged, as well as is funding from the National Science Foundation (CHE-0315337). K.H.P. also acknowledges support from the DOE, Los Alamos National Laboratory, Grant # 97831-001-04 4V.

Supporting Information Available: X-ray crystallographic file in CIF format for the structure determination of compound **B**. This material is available free of charge via the Internet at http://pubs.acs.org.

IC0503028